Cancer Gene Therapy (2010) 17, 780–791

www.nature.com/cgt

ORIGINAL ARTICLE

Enhanced target gene knockdown by a bifunctional shRNA: a novel approach of RNA interference

DD Rao[1], PB Maples[1], N Senzer[1,2,3,4], P Kumar[1], Z Wang[1], BO Pappen[1], Y Yu[1], C Haddock[1], C Jay[1], AP Phadke[1], S Chen[1], J Kuhn[5], D Dylewski[6], S Scott[6], D Monsma[6], C Webb[6], A Tong[1], D Shanahan[1,2] and J Nemunaitis[1,2,3,4]

[1]Gradalis, Inc., Dallas, TX, USA; [2]Mary Crowley Cancer Research Centers, Dallas, TX, USA; [3]Texas Oncology PA, Dallas, TX, USA; [4]Baylor Sammons Cancer Center, Dallas, TX, USA; [5]General and Oncology Surgery Associates, Dallas, TX, USA and [6]Van Andel Research Institute, Grand Rapids, MI, USA

RNA interference (RNAi) is a natural cellular regulatory process that inhibits gene expression by transcriptional, post-transcriptional and translational mechanisms. Synthetic approaches that emulate this process (small interfering RNA (siRNA), short hairpin RNA (shRNA)) have been shown to be similarly effective in this regard. We developed a novel 'bifunctional' RNAi strategy, which further optimizes target gene knockdown outcome. A bifunctional construct (bi-sh-STMN1) was generated against Stathmin1, a critical tubulin modulator that is overexpressed in human cancers. The bifunctional construct is postulated to concurrently repress the translation of the target mRNA (cleavage-independent, mRNA sequestration and degradation) and degrade (through RNase H-like cleavage) post-transcriptional mRNA through cleavage-dependent activities. Bi-sh-STMN1 showed enhanced potency and durability in parallel comparisons with conventional shRNA and siRNAs targeting the same sequence. Enhanced STMN1 protein knockdown by bi-sh-STMN1 was accompanied by target site cleavage at the mRNA level showed by the rapid amplification of complementary DNA ends (RACE) assay. Bi-sh-STMN1 also showed knockdown kinetics at the mRNA level consistent with its multieffector silencing mechanisms. The bifunctional shRNA is a highly effective and advantageous approach mediating RNAi at concentrations significantly lower than conventional shRNA or siRNA. These results support further evaluations.
Cancer Gene Therapy (2010) **17,** 780–791; doi:10.1038/cgt.2010.35; published online 2 July 2010

Keywords: bifunctional; RNA interference; Stathmin1

Introduction

RNA interference (RNAi) is a natural cellular regulatory process capable of inhibiting transcriptional, post-transcriptional and translational mechanisms thereby modulating gene expression.[1–4] RNAi technology is commonly used in reverse genetics approaches to study gene function and to show targets of therapeutic potential in cancer.[5–7] Several synthetic methods of silencing gene expression integral to disease phenotype have been developed.[8,9] Short hairpin RNA (shRNA) transcribed from an expression vector intrinsically differs from synthetic double-stranded small interfering RNA (siRNA) with respect to intracellular trafficking and nucleotide preference[10] and can result in enhanced gene knockdown effects. Recently, the process of RNAi by endogenously expressed hairpin RNAs, known as microRNAs (miRNAs), has been shown in mammalian cells.[11] By integrating an siRNA motif in the context of the well-known miR30-scaffold, shRNA expressed from constructs of defined specificity against a target gene can be processed through the endogenous miRNA biogenesis pathway.[12]

Using a miR30-scaffold, we developed a novel 'bifunctional' (bi) RNAi strategy. We postulate that a bifunctional construct that concurrently induces translational repression (cleavage-independent mRNA sequestration and degradation) and cleavage-dependent post-transcriptional mRNA degradation can achieve more effective silencing in comparison with siRNA or conventional single-functional shRNA targeted to the same sequence. The bifunctional construct bi-sh-STMN1 is directed against Stathmin1 (STMN1), a gene target candidate that is overexpressed in human cancer lines and was shown by us to be differentially overexpressed in cancer patients, based on mRNA and protein couplet signals in tumor/normal tissue specimen analysis.[13] STMN1 is critically involved in mitotic spindle formation.[14,15] Previously, studies have shown that STMN1 knockdown by conventional siRNA resulted in G_2/M cell cycle arrest, inhibition

Correspondence: Dr J Nemunaitis, Mary Crowley Cancer Research Centers, 1700 Pacific Ave, Suite 1100, Dallas, TX 75201, USA.
E-mail: jnemunaitis@marycrowley.org
Received 17 August 2009; revised 3 March 2010; accepted 3 March 2010; published online 2 July 2010

of clonogenicity and markedly increased apoptosis.[15–17] STMN1 knockdown also produced an additive to synergistic interaction with chemotherapeutic agents such as the taxanes.[18–20]

The bi-sh-STMN1 incorporates two stem-loop structures in an expression construct promoting both cleavage-dependent and cleavage-independent RNA-induced silencing complex (RISC) assemblies thereby generating RISC-associated mature effector small RNAs with multiple independent gene silencing activities. On the basis of the observation that miRNAs are associated with both non-nucleolytic (Ago1, 3, 4) and nucleolytic Ago2-containing RISC and siRNAs with the nucleolytic Ago2, the novel bifunctional strategy specifically promotes the loading of miRNA-like effector molecules onto the cleavage-independent RISC as well as the accumulation of siRNA effector molecules by the cleavage-dependent (Ago2 containing) RISC.[21] The bifunctional design thermodynamically accommodates passenger strand departure through cleavage-dependent and cleavage-independent processes so the functionality of the effectors is, thereby, set by programmed passenger strand guided RISC loading rather than being dependent on the Ago protein distribution in the target cell. Insofar as the bifunctional construct uses a natural process (that is, miRNA biogenesis), the host RNA polymerase II complex can be used to allow expression of multiple bifunctional shRNAs targeting multiple key over-expressed genes in tumor with a single primary transcript transcribing from a RNA pol II promoter[22,23] structurally analogous to the miR17-92 cluster on chromosome 13 with 6 miRNAs expressed in a poly-cistronic manner.[24] In this proof of principle study, we showed effective target knockdown and significant dose advantage *in vitro* in tumor cell killing when compared with conventional shRNA and siRNA targeting the STMN1 target gene.

Materials and methods

Materials and cell lines

siRNAs were purchased from Ambion (Austin, TX), DNA oligos were purchased from Integrated DNA Technologies (Coralville, IA), restriction enzymes were obtained from New England BioLabs (Ipswich, MA). DNA sequencing was carried out by SeqWright (Houston, TX). HCT-116 (ATCC# CCL-247), MDA-MB-231, and SK-MEL-28 cell lines were obtained from ATCC (Manassas, VA). Cells were cultured under the condition recommended by ATCC. Early passage cells were used for experiments.

Construction of STMN1 uni-functional shRNA (pGBI-1, pGBI-3) and bifunctional shRNA (bi-sh-STMN1, or pGBI-2)

The bi-sh-STMN1 consists of two stem-loop structures with miR-30 backbone. The first stem-loop structure has a complete complementary guide strand and passenger strand, while the second stem-loop structure has two base pair mismatches at positions 11 and 12 of the passenger strand. The sequences for both stem-loop structures are as follows:

Complete matching strands (5′-AAGGATCCTGCTGTT GACAGTGAGCGCGGCACAAATGGCTGCCAAATAG TGAAGCCACAGATGTATTTGGCAGCCATTTGTG CCTTGCCTACTGCCTCGGAAGCTTTG-3′);

Strands with mismatches (5′-AAGGATCCTGCTGTT GACAGTGAGCGCGGCACAAATGATTGCCAAATA GTGAAGCCACAGATGTATTTGGCAGCCATTTGT GCCTTGCCTACTGCCTCGGAAGCTTTG-3′),

where underlined are nucleotide differences between complete match and mismatched strands.

Two stem-loop structures were synthesized independently with two pieces of synthetic oligonucleotides each with overlapping sequences and fill-in reaction with T4 DNA polymerase to complete the double-stranded DNA for restriction digest and insertion into the plasmids. Each stem-loop structure was individually inserted into pSilencer vector between *Bam*HI and *Hind*III sites (Ambion). To join the two shRNA expression units, the *Hind*III site at the 3′ end of the stem-loop structure with complete matching strands expression unit was changed into a *Bgl*II site (5′-TGAGATCTCCGAGGCAGTAGGCA-3′) and the *Bam*HI site at the 5′ end of the mismatching strands expression unit was then joined to the 3′ end of strands with complete matching expression unit through the *Bgl*II site to establish the bifunctional expression unit.

To move the shRNA expression units from pSilencer into pUMVC3 vector, PCR primer was used to change the *Bam*HI sites to *Sal*I site (*Bam*HI to *Sal*I primer, 5′-AA GTCGACTGCTGTTGACAGTG-3′), PCR amplification with F seq primer (5′-AGGCGATTAAGTTGGG TA-3′), and the resulting PCR fragments were digested with *Sal*I and *Not*I and inserted into the *Sal*I and *Not*I sites of pUMVC3.

Sequence confirmation and vector production

The insert sequences were confirmed by sequencing from both directions with primers flanking the insert. The sequencing was performed by SeqWright.

For small-scale production, vector DNA were purified from *Escherichia coli* by EndoFree Plasmid Maxi kit (Qiagen, Valencia, CA). Purified plasmid DNA was quantified with Nanodrop ND-100 spectrophotometer (NanoDrop, Willmington, DE). Large-scale production of the Good Laboratory Practice quality plasmid DNA were contract produced by Aldevron (Fargo, ND). The inserts of Good Laboratory Practice-produced plasmids were also sequence confirmed.

Transfection of cell lines with siRNA or shRNA

Reverse transfection of cell lines was carried out with siPort NeoFX (Ambion) for siRNA or siPort Amine (Ambion) for shRNA by following the protocol recommended by the manufacturer. Transfection efficiency was routinely monitored by a green fluorescent protein expression vector and percentage green fluorescent protein-positive cells scored by flow cytometry analysis. Briefly, 1 h before transfection, healthy growing adherent cells were trypsinized and re-suspended in normal growth

medium at 1×10^5 cells ml^{-1}. siPORT NeoFX (or Amine) (5 μl per well) was diluted into a predetermined volume of Opti-MEM 1 medium (100 μl per well) for each six-well plate used and incubated for 10 min at room temperature. siRNA (plasmid DNA) was diluted into Opti-MEM 1 medium for a final concentration of 10–30 nM (1–3 μg ml^{-1} for shRNA), as required, in 100 μl per well volume of OptiMEM1. The diluted siPORT NeoFX (or Amine) and the diluted RNA (or plasmid DNA) were combined and incubated 10 min at room temperature. The transfection complexes were then dispensed into the empty six-well plates (200 μl per well). The trypsinized cells prepared earlier were gently mixed and 2.3 ml of the 1×10^5 cells ml^{-1} were overlayed into each well of the six-well plates, which were gently rocked back and forth to evenly distribute the complexes. The final volume of transfection was 2.5 ml per well. Incubation was performed at 37 °C checking after 8 h for any cytotoxicity. If Cytotoxicity was noticed, the media was replaced with fresh media. Fresh media was replaced after 24 h. The cells were assayed at 24, 48 h and 4 days after transfection for protein knockdown by Western, flow-cytometry or reverse transcription-polymerase chain reaction (RT-PCR). Transfections were also carried out with Transfectamine 2000 (Invitrogen, Carlsbad, CA) with the protocol recommended by the manufacturer.

RNA isolation

Total cellular RNA isolation was accomplished with RNeazy mini-kit (Qiagen) or with *mir*Vana miRNA isolation kit (Ambion) by following manufacturer's recommendations.

Stem-loop RT-PCR

Stem-loop RT primers specific for passenger strand or guide strand, PCR primers for passenger strands, PCR primer for guide strand and PCR primer for stem-loop RT primer are as follows: stem-loop RT primer for passenger strand (5′-GTCGTATCCAGTGCAGGGT CCGAGGTATTCGCACTGGATACGACTTTGGC-3′); stem-loop RT primer for guide strand (5′-GTCGTATCC AGTGCAGGGTCCGAGGTATTCGCACTGGATACG ACAAGGCA-3′); PCR primer for stem-loop (5′-GTG CAGGGTCCGAGGT-3′); PCR primer for guide strand (5′-GCCCTTTGGCAGCCATTTG-3′); PCR primer for matching passenger strand (5′-GCCCGGCACAAATGG CTG-3′); PCR primer for mis-match passenger strand (5′-GCCCGGCACAAATGATTG-3′). All primers were purchased from IDTDNA (IDTDNA; Coralville, IA). RT was carried out using the stem-loop RT primer and the SuperScript II Reverse Transcription Kit (Invitrogen) according to the manufacturer's protocol to create complementary DNA (cDNA) from total cellular RNA. The cDNA was then amplified by PCR (GoTaq Kit, Promega, Madison, WI) with a denaturation at 94 °C for 2 min; 30 cycles of 94 °C for 30 s, 50 °C for 30 s and 72 °C for 1 min; 72 °C for 5 min and a final hold of 4 °C. PCR products are run on a 4% agarose gel and ultraviolet images were captured by G-Box imaging system (Syngene, Frederick, MD).

5′ RACE

The 5′ rapid amplification of cDNA ends (5′RACE) assay was performed using GeneRacer kit (Invitrogen) with gene-specific primers: STMN1 RT primer (5′-TATGG CAGGAAAGGATGAGG-3′); STMN1 PCR primer 1 (5′-CAGAGCCAATACAGTACATGCC-3′); STMN1 PCR primer 2 (5′-GATCTGGATCTACCTATACAG TCC-3′). Total cellular RNA was added to RNA oligo, and mixed with ligase buffer, RNase Out and T4 RNA ligase. Ethanol precipitated samples were suspended in nuclease-free H_2O for RT by Superscript III (Invitrogen) with STMN1 gene-specific RT primer. After RT, 1/20 of cDNA were used for first PCR amplification by GoTaq (Promega) with GeneRacer PCR primer and STMN 1 gene-specific primer 1 by touchdown PCR for 30 cycles. In all, 1/50 of the first round of PCR was then subject to additional 30 cycles of PCR with nested primers (GeneRacer nest 5′ PCR primer and STMN1 gene-specific primer 2).

Quantitative RT-PCR

In all, 1 μg of isolated total cellular RNA was converted to cDNA using oligo dT primer in a 20 μl reaction with Superscript III First-Strand Synthesis System (Invitrogen). The synthesized cDNA was diluted 100-fold and 5 μl of diluted cDNA was amplified in a 25 μl QPCR reaction with SyberGreen in a iQ5 Multicolor Real-Time PCR Detection System (Bio-Rad, Hercules, CA). A pair of PCR primers was designed to span the predicted cleavage site of STMN1 so as to measure pGBI-2-mediated knockdown of STMN1 mRNA (forward primer: 5′-TG GCAGAAGAGAAACTGACCCACA-3′; reverse primer: 5′-TCGTCAGCAGGGTCTTTGGATTCT-3′). Glyceraldehyde 3-phosphate dehydrogenase (forward primer: 5′-CGACCACTTTGTCAAGCTCA-3′; reverse primer: 5′-CGACCACTTTGTCAAGCTCA-3′) was used as internal control to normalize STMN1 gene expression with ΔΔCt method to analyze the relative STMN1 gene expression. All samples treated with either pGBI-1, pGBI-2 or pGBI-3 was compared with media-control samples and the changes of STMN1 expression were presented as percentage of media-control.

Flow cytometry analysis

Transfected or untransfected cells were washed, trypsinized and collected. A small aliquot is removed for a cell count. In all, 1×10^6 cells were then pelleted and resuspended in 500 μl of Cyto Fix and Perm solution (BD Biosciences, Rockville, MD) for 10 min at room temperature. After 10 min, cells were washed with 1 ml of PermWash. After wash, the pellet is resuspended in 300 μl of PermWash buffer and divided into three tubes of 100 μl each. One tube was for unstained control, second tube was for isotype control. Third tube was for rabbit anti-human STMN1 (purified antibody) followed by secondary goat anti-rabbit IgG (phycoerythrin), or rabbit anti-human β-actin followed by secondary goat anti-rabbit IgG (phycoerythrin). In total, 10 μl of primary antibody was used for each sample and incubated at 4 °C for 30 min, followed by a rinse with 1 ml of PermWash

buffer, incubated with 10 μl per sample of the phycoerythrin-labeled secondary antibody for 10 min at 4 °C in the dark. After tagging the cells with secondary antibody, the cells are washed 2 × with 1.0 ml of PermWash. After the last wash, the cells were resuspended in Staining Buffer and read using the fluorescence-activated cell sorting Caliber (BD Biosciences) and data analyzed using CellQuest Pro software (BD Biosciences) to quantify the STMN1 or β-actin stained cells.

Western immunoblotting

Cells were lysed with lysis buffer CellLytic-M and scraped off the surface of the culture dish incubate at room temperature for 30 min on a slow shaker, and briefly centrifuged. A small aliquot for protein concentration estimation by Coomassie Bradford Plus Assay was taken with bovine serum albumin as standard. The SoftMaxPro software (Molecular Devices, Sunnyvale, CA) was used to calculate the values and plot the standard curve. Equal amounts of protein were separated on a pre-assembled gel (usually 5–20 μg) 15% polyacrylamide gel electrophoresis using Mini-Protein II Cell system (Bio-Rad). After electrophoresis, the separated proteins were electro-transferred on to a polyvinylidene fluoride membrane with standard condition. Transferred membranes were first blocked with blocking buffer containing 5% non-fat dried milk in Dulbecco's phosphate buffered saline overnight at 4 °C. After two changes of wash buffer, proteins were tagged first with determined dilution of primary antibody and then horseradish peroxidase-conjugated secondary antibody. Chemiluminescent detection was carried out by ECL plus western blotting detection reagents with G:BOX Chemi XT16 automated chemiluminescence image analyzer (Syngene, Frederick, MD). Membranes can be stripped and re-probed with a different antibody or house keeping protein such as β-actin.

Viable cell count

The cell numbers of transfected and untransfected control were determined by EasyCount System (Immunicon, Huntingdon Valley, PA). The EasyCount System, together with the EasyCount ViaSure Kit, provides automated counting of live and dead nucleated cells. Briefly, the tissue culture cells were trypsinized to prepare cell suspensions in growth medium. In total, 25 μl of cell suspensions and 25 μl of fluorescent staining reagent were gently mixed. In all, 10 μl of the mixture were loaded to the EasyCount slide and the total cells and the viable cells were measured by EasyCount device.

Statistical analysis

All data analyses were performed using SPSS 13.0 (SPSS Inc., Chicago, IL). One-way analysis of variance was performed to see if there were any differences in cell survival between low, medium and high doses of bi-sh-STMN1 and untreated cells for cell cycle analysis. *Post hoc* comparisons were made using the Tukey's Honestly Significant Difference test to identify wherein mean cell survival differences occurred between the varying treated and untreated cells. Similar analysis was applied to siRNA, shRNA and bi shRNA comparisons. A repeated-measures analysis of variance, followed by a Tukey's Honestly Significant Difference *post hoc* test, was performed to look for differences in the kinetics of cell survival at various doses of siRNA, shRNA and bi shRNA over time after transfection.

Results

Vector design and cell line selection for in vitro *studies*

The design of the bifunctional expression vector incorporated both cleavage-dependent and cleavage-independent structural components (Figure 1a) designed to promote differential RISC assembly and, consequently, produce Ago 2 and non-nucleolytic Ago protein effectors directed against the same target sequence on STMN1 mRNA.[25] To the point, translational repression by siRNAs with full complementarity to reporter mRNA can occur independent of Ago 2.[25] The cleavage-dependent component requires complete matching sequences of the passenger and guide strands for optimal activity. After processing by the RNase III enzyme Dicer, the double-stranded RNA is bound by the RISC loading complex (RISC loading complex incorporating Dicer, TRBP and AGO2) and the passenger strand is cleaved by the RNase H-like activity of Ago 2 (encoded by its P-element induced wimpy testis in *Drosophila* domain) liberating the guide strand which, as a component of RISC binds to and cleaves complementary target mRNA (cleavage-dependent process). In addition, our bifunctional vector incorporates a cleavage-independent component, which contains mismatches between the passenger and guide strands at the ostensible cleavage site resulting in a lower thermodynamic stability that promotes the dissociation of the passenger strand through a cleavage-independent process.[26,27] This component will in effect be loaded onto non-nucleolytic Ago protein RISCs and function through mRNA sequestration and translation repression.[11]

The expression unit for the bifunctional shRNA to Stathmin1 (bi-sh-STMN1) is inserted between the *Sal*I and *Not*I sites of mammalian expression vector pUMVC3 (Figure 1b) and is driven from an enhanced (pol II) cytomegalovirus promoter.[28] It contains two stem-loop structures in a previously described miR-30 backbone,[12] one with complete matching passenger and guide strands (cleavage-dependent), and the other with 2-bp mismatches between passenger and guide strands (cleavage-independent). The GC to AU switches are at positions 11 and 12 of the passenger strand, which create mismatches at the central location similar to most miRNAs[26] (predicted secondary structure shown on Figure 1c).

The STMN1 mRNA target site we selected was based on maximal knockdown efficacy as determined by comparison of several commercially available siRNA^{STMN1}s. The selected target site was also screened with the Basic Local Alignment Search Tool local alignment program to limit the potential matches or 'seed sequence' matches with other human transcripts. For comparative purposes and for

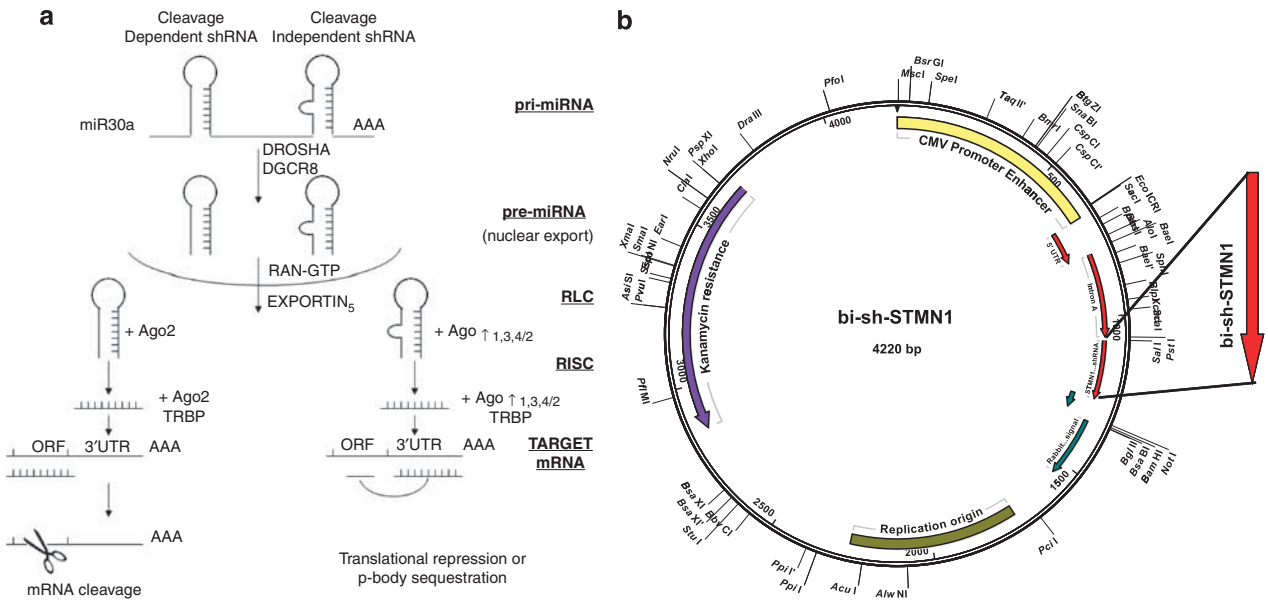

c

Plasmids	shRNA Sequence	Predicted Mechanism
pGBI-1	GGAUCCU G GA C GUGAAG GCU UUGA CAGU GCG GGCACAAAUGGCUGCCAAAUA CCA CGA GGCU GUCA CGU CCGUGUUUACCGACGGUUUAU GUUU A CC UC U GUAGAC	Cleavage Dependent
bi-sh-STMN1	GGAUCCU G GA C GUGAAG GCU UUGA CAGU GCG GGCACAAAUGGCUGCCAAAUA CCA GGCU GUCA CGU CCGUGUUUACCGACGGUUUAU CC UC U GUAGAC XbaI G GA C AU GUGAAG GCU UUGA CAGU GCG GGCACAAAUG UGCCAAAUA CCA CGA GGCU GUCA CGU CCGUGUUUAC ACGGUUUAU GUUU A CC UC U CG GUAGAC	Bi-functional
pGBI-3	GGAUCCU G GA C AU GUGAAG GCU UUGA CAGU GCG GGCACAAAUG UGCCAAAUA CCA CGA GGCU GUCA CGU CCGUGUUUAC ACGGUUUAU GUUU A CC UC U CG GUAGAC	Cleavage Independent

Figure 1 The concept of a novel approach for RNAi and the expression constructs. (**a**) Schematic diagram illustrates simultaneous bifunctional mechanism through cleavage-dependent and -independent pathways. (**b**) Circular diagram of expression constructs for shRNA expression. pUMVC3 vector's mammalian expression unit contains enhanced cytomegalovirus (CMV) promoter with CMV IE 5′ UTR and partial IE Intron A and rabbit β-globin poly A site. The shRNA expression unit is inserted in the multiple cloning sites between the CMV IE Intron A and rabbit β-globin poly A sites. (**c**) shRNA sequences inserted into the multiple cloning sites of pUMVC3 for bi-sh-STMN1 (pGBI-2), pGBI-1 (cleavage-dependent component) and pGBI-3 (cleavage-independent component).

consistency, the selected STMN1 mRNA target site was used for siRNA and for all shRNA expression constructs throughout this study. To test whether the STMN1 expression could be effectively knocked down with each of the separate components of the bi-sh-STMN1 construct, CCL-247 cells were transfected with either 1, 2 or 3 μg ml^{-1} of the pGBI-1 (cleavage-dependent component) or of the pGBI-3 (cleavage-independent component) plasmid. Both effectors at all three doses knocked down STMN1 protein expression at 48 h after transfection (data not shown).

For *in vitro* study, we chose to show activity in cell lines overexpressive of STMN1 protein. As such, we compared a battery of cell lines and found a wide variation of STMN1 protein expression, which could be grouped into low, medium and high STMN1-expressing cells by normalizing to STMN1 expression in peripheral blood cells (with lowest STMN1 expression); low STMN1-expressing cells are less than fivefold elevated from peripheral blood cells, medium-expressing cells are <20-fold elevated, while high-expressing cells are >20-fold elevated in comparative expression (data not shown). Two medium STMN1-expressing cell lines, colon cancer cell line CCL-247 and melanoma cell line SK-MEL-28 and a high STMN1-expressing cell line, breast cancer cell line MDA-MB-231 were selected for our *in vitro* studies.

Detection of product effector molecules

Insofar as the bifunctional construct (bi-sh-STMN1; pGBI-2) consists of two stem-loop structures of similar sequence in tandem (Figure 1c), we first sought to confirm the effective synthesis and maturation of both types of effector molecules in the bi-sh-STMN1-transfected cells. Using an adapted highly sensitive and specific stem-loop RT-PCR method that was developed to detect

miRNAs,[28] we confirmed that the guide strands derived from the bi-sh-STMN1 were as predicted (Figure 2a, lane 4, black arrow). The guide strand sequence was shown in RNA isolated from cells transfected with either bi-sh-STMN1 or siRNA^{STMN1} (Figure 2a, lane 5, black arrow). An additional minor PCR product was detected from the bi-sh-STMN1-transfected cells (Figure 2a, lane 4 red arrow), which was sequenced and shown to be a processing intermediate containing 11 bases of the miR30 stem sequence. The guide strand was not detected either from RNA isolated from un-transected cells (Figure 2a, lane 2) or from scrambled shRNA-transfected cells (Figure 2a, lane 3).

Using primers specific either for the matched or mismatched passenger strands, we further confirmed that both matched and mismatched passenger strands were present in the bi-sh-STMN1-transfected cells (Figure 2b, lane 4 for matched passenger strand, lane 9 for mismatched passenger strand), whereas only the fully matching passenger strand was detected from the siRNA^{STMN1}-transfected cells (Figure 2b, lane 5). No RT-PCR product was detected from untransfected cells or cells transfected with scrambled shRNA. These findings support our premise that mature, cleavage-dependent and -independent effectors were produced after bi-sh-STMN1 transfection.

Validation of target site cleavage

The cleavage-dependent component of the bi-sh-STMN1 construct should be able to induce STMN1 target site cleavage. The 5′ RACE method was used to validate target site cleavage as predicted from the cleavage-dependent siRNA component of bi-sh-STMN1.[29] We designed gene-specific primers both for RT and for PCR. For PCR, we also used the gene-specific nested primer strategy to reduce any nonspecific background. The RACE PCR product with predicted size was detected in cells transfected with either bi-sh-STMN1 or siRNA^{STMN1} (Figure 3, lanes 4 or 5, respectively, red arrow), and was confirmed by DNA sequencing to represent a STMN1 mRNA fragment after cleavage between nucleotide position 10 and 11 of the sense strand.

STMN1 protein knockdown

To show the specificity of target protein knockdown, after transfection with bi-sh-STMN1, CCL-247 cells were tagged with STMN1-specific antibody for flow cytometry analysis. At 48 h after transfection, flow cytometry analysis showed 93% reduction in STMN1 protein expression (shift in fluorescent intensity, Figure 4, upper panels) as compared with untreated control. By contrast, treatment with the scramble control did not result in STMN1 reduction. β-Actin expression was not changed by bi-sh-STMN1 treatment (Figure 4, lower panels).

Comparative STMN1 protein knockdown and mRNA knockdown kinetics

Comparative STMN1 protein expression was assessed by western immunoblot. At 48 h after transfection of SK-MEL-28 cells, the bi-sh-STMN1 (pGBI-2) is the most

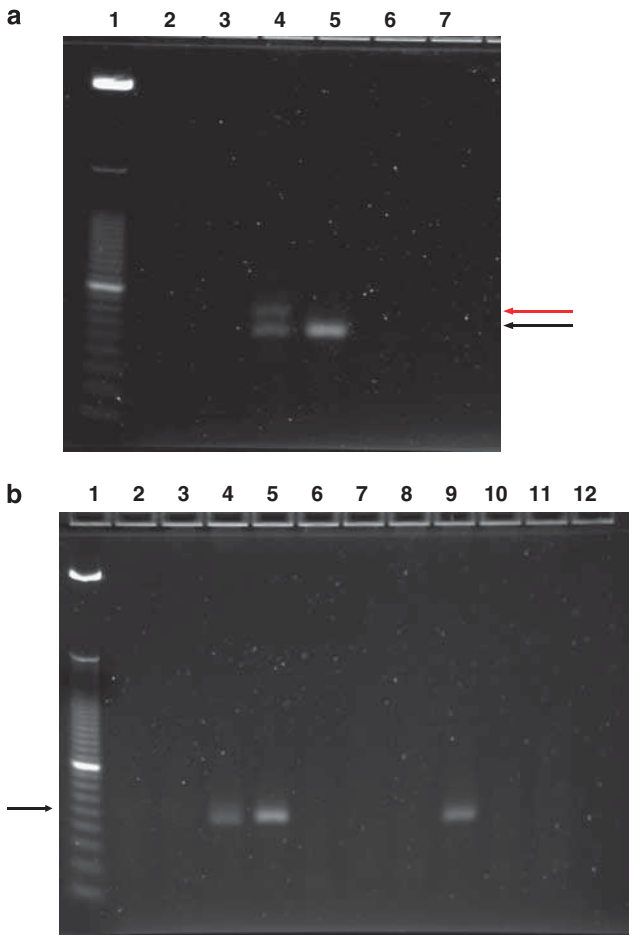

Figure 2 Both passenger and guide strands of the mature shRNA are detected from bi-sh-STMN1-transfected CCL-247 colon cancer cells. (**a**) Photo-image of agarose gel showing the RT-PCR product of the guide (antisense) strand (black arrow). This sequence was confirmed. Total cellular RNA was first reverse-transcribed with guide strand-specific stem-loop RT primer and subsequently amplified with the guide strand-specific and stem-loop-specific PCR primer set. PCR amplified products were run onto a 4% agarose gel and stained with ethidium bromide and visualized under ultraviolet (UV) light. The red arrow indicates a processing intermediate, containing 11 bases of the miR30 stem (sequence confirmed by SeqWright). Lane 1: size marker. Lane 2: no transfection. Lane 3: transfected with scramble control. Lane 4: transfected with bi-sh-STMN1. Lane 5: transfected with siRNA^{STMN1}. Lane 6: no RT control. Lane 7: no PCR primer control. (**b**) Photo-image of agarose gel showing the RT-PCR product of the passenger (sense) strand (black arrow). Total cellular RNA was reverse-transcribed with passenger strand-specific stem-loop RT primer for cDNA synthesis. Two primer sets were used to differentiate shRNA with or without mismatches. cDNA was amplified with passenger strand-specific primers either for the complete match passenger strand (lanes 2–6) or for passenger strand with mismatches (lanes 7–11) and stem-loop-specific PCR primer sets. PCR amplified products were run onto a 4% agarose gel and stained with ethidium bromide and visualized under ultraviolet (UV) light. The amplified PCR products were sequence confirmed. Lanes 2 and 7: no transfection. Lanes 3 and 8: transfected with scramble control. Lanes 4 and 9: transfected with bi-sh-STMN1. Lanes 5 and 10: transfected with siRNA^{STMN1}. Lanes 6 and 11: no RT control. Lane 12: water control.

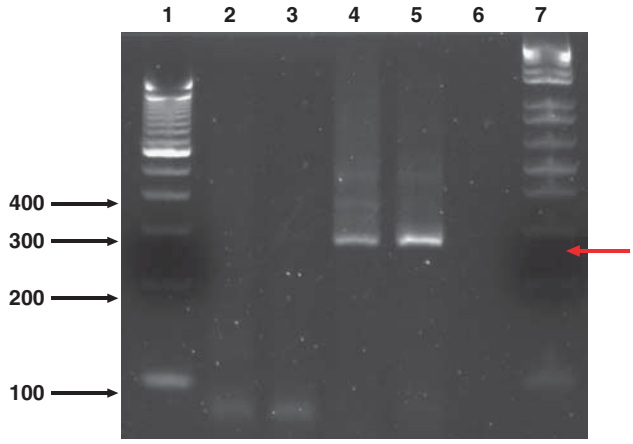

Figure 3 STMN1 mRNA target site cleavage is detected from the bi-sh-STMN1-transfected CCL-247 cells by 5′ RACE. Photo-image of agarose gel resolving RACE-PCR products. RACE-PCR products were detected in cells transfected with either bi-sh-STMN1 or siRNA^{STMN1}. CCL-247 cells were transfected with 7.22×10^{-13} M of bi-sh-STMN1 (lane 4), or 30 nM of siRNA (lane 5); a 285-bp PCR product was detected (red arrow). Lane 1 is 100-bp size marker, lane 2 is RNA from untransfected cells. Lane 3 is RNA from scramble shRNA-transfected cells. Lane 6 is PCR only control. Lane 7 is 1 kb size marker.

effective in STMN1 knockdown when compared with either pGBI-1 or pGBI-3 (44, 29 and 11% knockdown, respectively) (Figure 5a).

We also evaluated the mRNA knockdown kinetics of the composite bifunctional construct (pGBI-2) compared with constructs comprised each of the individual components using SK-MEL-28 cells. Figure 5b illustrates the comparative target mRNA knockdown kinetics over the 72 h after exposure to pGBI-1, -3 and bi-sh-STMN1 (pBGI-2) as determined by quantitative RT-PCR. The quantitative RT-PCR primers were designed to flank the target site for the most effective detection of target site cleavage-mediated STMN1 mRNA knockdown. pGBI-1 (cleavage-dependent mRNA degradation only) induced STMN1 mRNA knockdown was evident at 24 h, peaking at 48 h. By comparison, with pGBI-3 treatment (through translational inhibition and/or sequestration in the p-body with or without subsequent mRNA deadenylation, decapping and degradation, in spite of the same target sequence)[30,31] STMN1 mRNA was more abundant at 24 and 48 h compared with the untreated cells and started to decline only at 72 h after transfection. The STMN1 mRNA knockdown response to the bi-sh-STMN1 (pGBI-2) was evident at 48 h and continued to increase at 72 h. We could not ascertain changes at later time

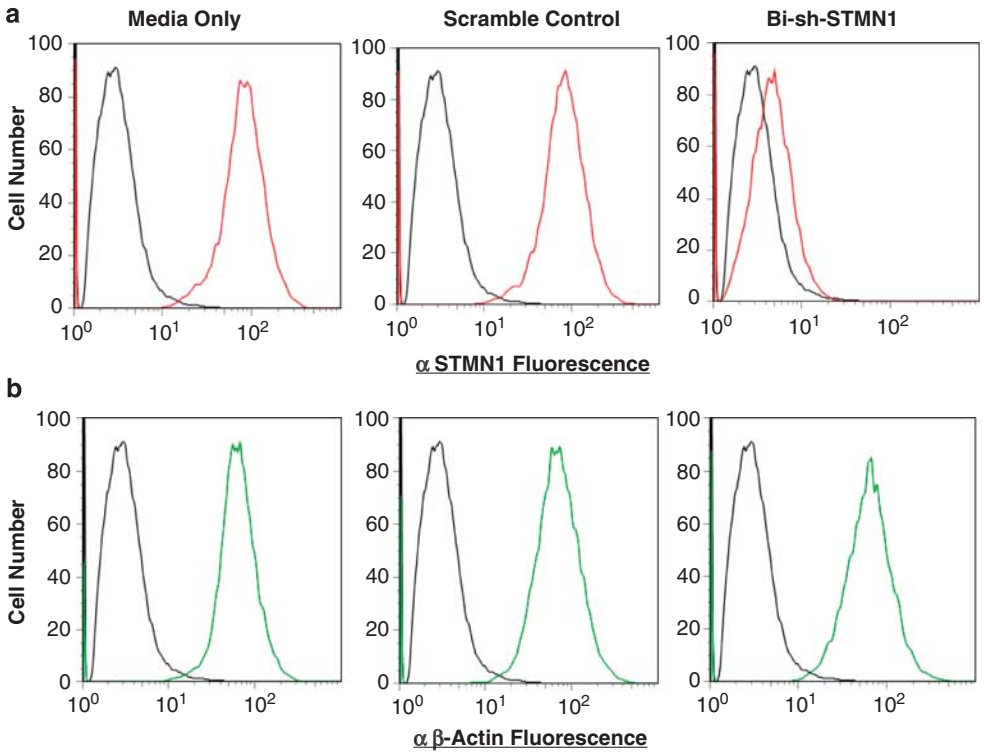

Figure 4 bi-sh-STMN1 effectively knocks down STMN1 protein expression in CCL-247 cells. CCL-247 cells were transfected with 3 μg ml^{-1} of bi-sh-STMN1. At 48 h after transfection, transfected cells were harvested for immuno-stain with either STMN-specific primary antibody (upper panels) or β-actin-specific primary antibody (lower panels). The antibody tagged cells were analyzed by flow cytometry. The result is shown; black line is secondary antibody (phycoerythrin-conjugated antibody) fluorescence, the green line is STMN1-specific fluorescence and the red line is β-actin-specific fluorescence.

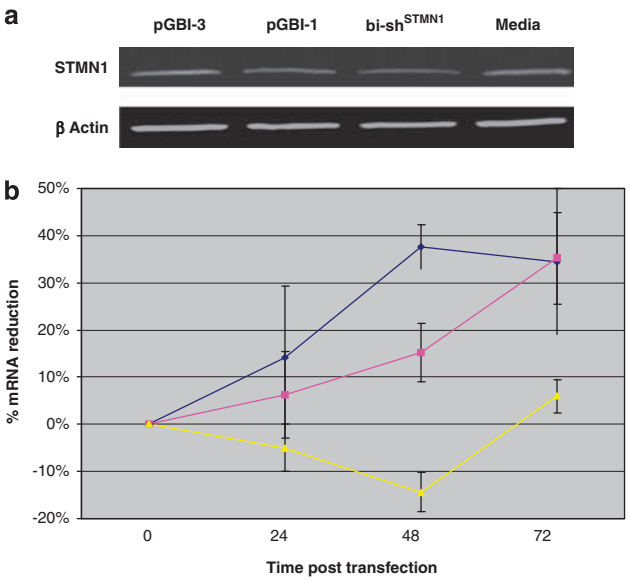

Figure 5 STMN1 mRNA knockdown kinetics. SK-MEL-28 cells were reverse-transfected with pGBI-1 (complete matching), or pGBI-2 (bifunctional) or pGBI-3 (with mismatches) at 1 μg ml^{-1} concentration. (**a**) At 48 h after transfection, cells were harvested and extracted for protein. Equal amount of total cell protein were loaded onto a 15% polyacrylamide gel electrophoresis (PAGE) for western immunoblot. Photo-image of the result of western immunoblot detect STMN1 and β-actin with either STMN1- or β-actin-specific antibody. (**b**) At 24, 48 and 72 h after transfection, STMN1 mRNA level were determined by quantitative reverse transcriptase (qRT)-PCR method normalized to the internal glyceraldehyde 3-phosphate dehydrogenase (GAPDH) mRNA level and percent reduction in STMN1 mRNA were compared with untransfected cells. pGBI-1 (complete matching, blue line), or pGBI-2 (bifunctional, red line) or pGBI-3 (with mismatches, yellow line).

points because of the limitations of the *in vitro* transfection system (untransfected cell growth).

Cancer cell growth inhibition

There was a dose-response pattern of CCL-247 cell survival after treatment with all three constructs; the bi-sh-STMN1 with an IC_{50} of 1.81×10^{-13} M at 24 h, pGBI-1 with an IC_{50} of 3.61×10^{-13} M and pGBI-3 with an IC_{50} of 7.22×10^{-13} M (Figure 6a). Additional cell survival results with bi-sh-STMN1 were shown with MDA-MB-231 and SK-MEL-28 cells; the dose requirements for cancer cell growth inhibition were observed to differ between the cell lines (data not shown). The dose-response data suggested an advantage of the bi-sh-STMN1 over pGBI-1 and pGBI-3 at the low-dose range (10^{-13}–10^{-14} M range, Figure 6a). We next examined the bi-sh-STMN1 construct's effect on cancer cell growth inhibition over 72 h as compared with each of it's individual components (pGBI-1 and pGBI-3) at three different doses that are lower than the IC_{50} for the bifunctional with 3.61×10^{-13} M as the highest dose and two additional lower doses (9.02×10^{-14} and 2.26×10^{-14} M). Reverse transfection of CCL-247 cells was performed with the three different concentrations for each construct. At the highest concentration (3.61×10^{-13} M), all three constructs inhibited cancer cell growth equally (data not shown). At the 9.02×10^{-14} M, all three constructs were observed to significantly inhibit CCL-247 growth for the 3-day period when compared with the no treatment control (Figure 6b), but the bi-sh-STMN1 construct was able to sustain growth inhibition more effectively through day 3 when compared with the single component construct (pGBI-2 vs pGBI-1, $P = 0.002$; pGBI-2 vs pGBI-3, $P = 0.003$). Even at the lowest dose (2.26×10^{-14} M), bi-sh-STMN1 showed a significant difference in growth inhibition compared with both the individual cleavage-dependent (pGBI-1) and -independent (pGBI-3) constructs (bi-sh-STMN1 vs pGBI-1, $P < 0.001$, bi-sh-STMN1 vs pGBI-3, $P < 0.001$) (Figure 6c).

Compare bi-sh-STMN1 with its siRNA counterpart

We next compared the performance of bi-sh-STMN1 with siRNA^{STMN1}. CCL-247 cell growth inhibition was monitored over a wide range of concentrations of siRNA^{STMN1} and compared with the dose response of bi-sh-STMN1. The bi-sh-STMN1 resulted in significantly greater tumor cell kill (lower percent survival) than the siRNA ($P = 0.004$) (Figure 7). Using the 5′ RACE method the target-specific cleavage product was readily detected at essentially all siRNA concentrations, while the cleavage product was only detected at the higher dose of bi-sh-STMN1 (Figure 7), thereby supporting an additional non-cleavage-dependent mechanism of action consistent with bi-sh-STMN1 design.

Discussion

The miR-30 backbone used in our design is reported to undergo a biogenesis process similar to endogenous miRNA.[12] The primary transcripts of endogenous miRNAs are synthesized from genomic DNA in the nucleus as long RNA strands with hairpin structures, which are further processed to mature 21–23 bp double-stranded miRNA through a series of RNase III enzyme digests. The maturation process involves at least two RNase III enzyme complexes; first, the Drosha/DGCR8 microprocessor complex produces the pre-miRNA hairpin structure which, after nuclear export through Exportin 5, is incorporated into the RISC loading complex in which the second enzyme, Dicer, excises the loop producing the mature miRNA,[32] which is the effector molecule that is loaded onto RISC for RNAi.[33] As previously noted, the differential distribution of non-nucleolytic (Ago1, 3, 4) and nucleolytic Ago2 (↑Ago1, 3, 4/Ago2) in the cleavage-independent RISC (miRNA-like) and the specific accumulation of Ago2 protein in the cleavage-dependent RISC (siRNA)[21] determine the functionality of the effectors. To determine if our designed bi-sh-STMN1 is accurately processing and successfully producing both types of the mature effector molecules (double-stranded RNA with 3′ overhangs and complete matching strands and double-stranded RNA with 3′ overhangs and specified mismatches), we adapted the RT-PCR method developed for miRNA[34] to detect

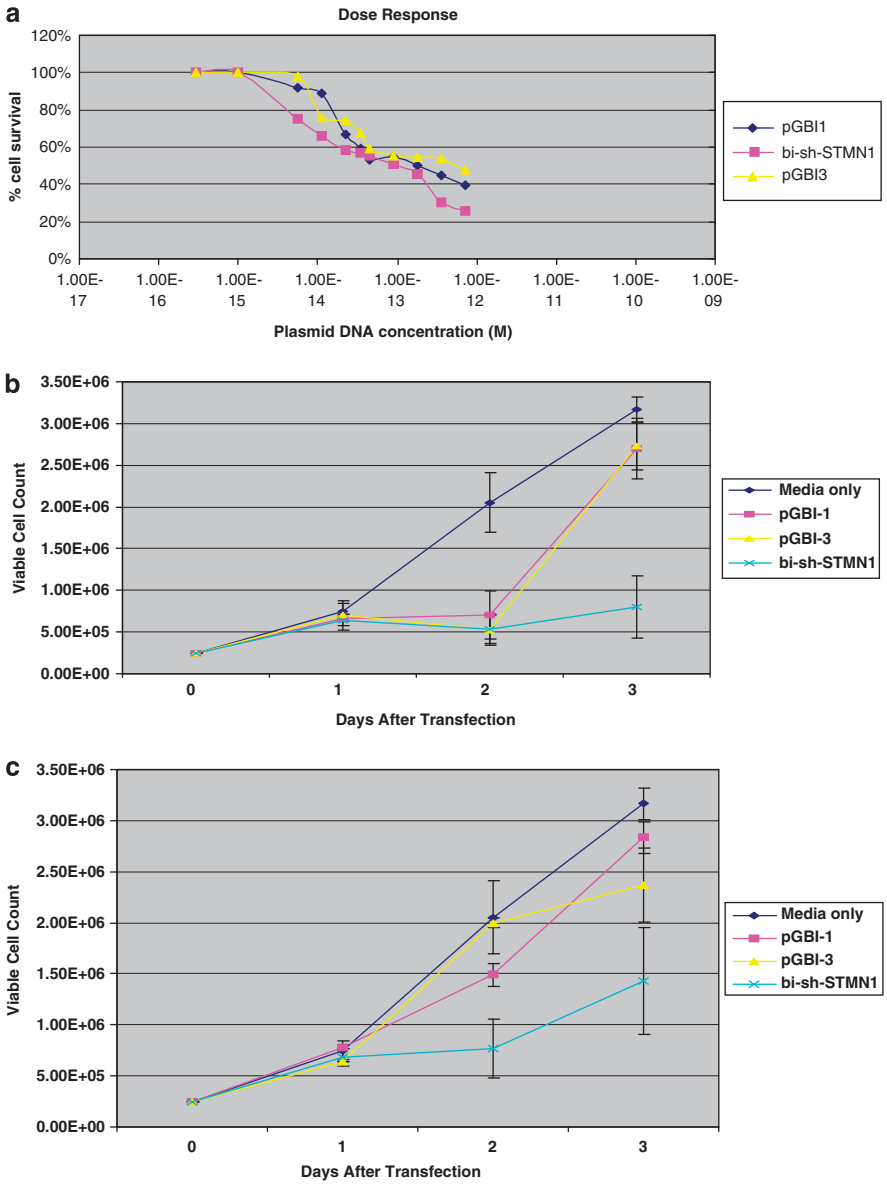

Figure 6 Dosing advantage of bi-sh-STMN1 when compared with cleavage-dependent (pGBI-1) and cleavage-independent (pGBI-3) components. (**a**) Dose-response curve for bi-sh-STMN1, pGBI-1 and pGBI-3. The *x* axis is increasing dose of plasmid concentration from left to right. The *y* axis is viable cell number counted after 24 h of treatment. Each data point represents the average of triplicate of samples with s.d. The concentration range of bi-sh-STMN1, pGBI-1 and pGBI-3 varied from 1.44×10^{-12} to 5.63×10^{-15} M. (**b**, **c**) Viable cell counts after bi-sh-STMN1 (light blue lines) transfection was compared with the constructs with the single cleavage-dependent (pGBI-1, red lines) and -independent (pGBI-3, yellow lines) shRNA elements. CCL-247 cells were treated with two doses for each construct; 9.02×10^{-14} M, or 2.26×10^{-14} M in comparison with untransfected cells (dark blue lines). Each data point represents a mean of triplicate samples with s.d. (**b**) CCL-247 cells treated with 9.02×10^{-14} M of constructs. (**c**) CCL-247 cells treated with 2.26×10^{-14} M of constructs.

the designed mature miRNA/siRNA and to discriminate between matched and mismatched passenger strands.

Results confirmed the presence of the predicted mature cleavage-dependent/cleavage-independent components. Moreover, we confirmed that both matched and mismatched passenger strands were synthesized from the bi-sh-STMN1 cells whereas only the fully matching strand was detected for the $siRNA^{STMN1}$-transfected cells. It appeared that the mismatched passenger strand was present in higher steady-state quantities than the matched passenger strand, which is consistent with cleavage of the fully matching passenger strand by Ago 2. However, insofar as the analysis of the RT-PCR product by agarose gel electrophoresis is only semi-quantitative, quantitative studies with TaqMan probes will be required to further assess this finding. To additionally support the hypothesized mechanism of the bi-sh-STMN1, we used the

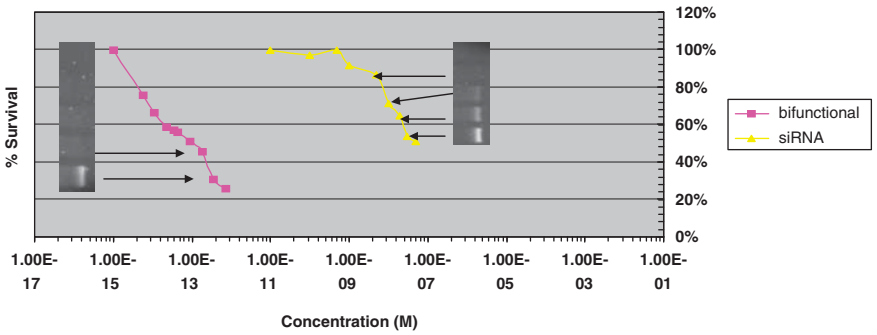

Figure 7 Correlation of STMN1 mRNA target cleavage and cell growth comparing bi-sh-STMN1 and siRNA^{STMN1}. A composite dose-response curve for bi-sh-STMN1 (red) and STMN1 siRNA (yellow) correlated with STMN1 mRNA cleavage. The *x* axis is increasing dose of plasmid/siRNA concentration from left to right. The *y* axis is percent cell survival after 24 h of treatment. Each data point represents the average of triplicate samples. The concentration range of bi-sh-STMN1 varied from 1.44×10^{-12} to 5.63×10^{-15} M. The concentration range for siRNA^{STMN1} varied from 5×10^{-7} to 1×10^{-10} M. Electropherogram inserts show 5′ RACE product detected from transfected CCL-247 cells indicating cleavage product.

5′ RACE method to confirm that the target cleavage site of the siRNA component of the bi-sh-STMN1 was the same as for siRNA^{STMN1}.

Involvement of both cleavage-dependent and -independent mechanisms in mediating the bi-sh-STMN1 function likely explains the close to maximum knockdown (93%) of STMN1 in CCL-247 tumor cells 48 h after the treatment as shown by flow cytometry. Using SK-MEL-28 cells, less efficient STMN1 knockdown was observed at 48 h by western immunoblot (Figure 5a, 44% for bi-sh-STMN1, 29% for pGBI-1 and 11% for pGBI-3) presumably because of differences in transfection efficacy and cell growth rate. However, in comparison with its individual cleavage-dependent and cleavage-independent components, the bi-sh-STMN1 produced the most efficient protein knockdown. Although bi-sh-STMN1 is the most efficient in protein knockdown, it is comparatively less efficient in target mRNA knockdown than pGBI-1 (cleavage-dependent component only) at 48 h as measured by quantitative RT-PCR. This observation is consistent with our suggested hypothesis that the bi-sh-STMN1 is, in effect, working through multiple RNAi pathways. During the initial 48 h of kinetics testing (Figure 5b), the bi-sh-STMN1 results in both mRNA degradation and sequestration, thus the bi-sh-STMN1 seems to be less effective than pGBI-1 in knockdown at the mRNA level. However, presumably, for the bi-sh-STMN1 (with both cleavage-dependent and -independent motifs), both mRNA cleavage (RNase H-like mechanism) and mRNA sequestration into the p-body initially occur followed at a later time by deadenylation-mediated decapping and mRNA degradation within the p-body, thereby appearing to be less efficient at target mRNA knockdown than pGBI-1 during the first 48 h, but producing additive STMN1 mRNA cleavage and degradation at a later time reflecting the temporal pattern of pGBI-3). Conversely, at the protein level (Figure 5a) as well as at the functional level (Figure 6b and c), the bifunctional seems to be more effective than either pGBI-1 or -3. Specifically, although the cleavage-dependent construct results in a 38% mRNA knockdown vs 15% by the bifunctional within the first 48 h after transfection, the bifunctional construct contemporaneously results in a 44% protein knockdown vs 29% by the cleavage-dependent construct. Given that complementary 3′-UTR specific miRNA mimics can effect mRNA degradation,[35] which could suggest that enhanced bifunctional efficacy is simply because of a siRNA dosing effect, the difference in pGBI-1- and pGBI-3-mediated mRNA knockdown kinetics show the differing mechanisms of action of the individual bifunctional components, which derives from differential Ago-containing RISC loading. We will further confirm the differential RISC loading using immunoprecipitation of each Ago protein-containing RISC at a later date.[21,36] Insofar as the same concentrations of plasmids used for all three constructs in this set of experiments, are expected to lodge the same number of plasmid copies in transfected cells and, therefore, the same number of primary transcripts under the same transfection conditions, the number of effector molecules are the same for each separate construct set. Thus, these data support the additive, if not synergistic, effect of the bifunctional construct.

Having evaluated an alternative effector mechanism and shown the functional efficacy of the bi-sh-STMN1 vector, we further examined anticancer activity *in vitro* and successfully showed effective cell kill in several cancer cell lines of different cancer types. Studies are underway to correlate STMN1 expression level in different cell types in relation to effective dose requirement.

We also compared bi-sh-STMN1 with siRNA directed against the same STMN1 target site. The bi-sh-STMN1 achieved an IC_{50} at 5 logs lower molar concentration than siRNA^{STMN1}. There is evidence of functional siRNA nuclear activity early after cell entry[37,38] and with subsequent nuclear exclusion of siRNA mediated by exportin 5 has been shown in human cells.[37,38] However, within 4 h after transfection, siRNA has completely relocated to the cytoplasm although at 48 h only 1% of initial delivered siRNA is available to mediate activity.[39] There are several strategies to modify siRNA to improve intracellular stability.[40] However, after vector-based

DNA achieves stability within the nucleus[41] and steadily produces shRNA through its pol II promoter, which allows for spatial and temporal control, thereby providing a continuous expression of inhibitory effectors with a prolonged functional half-life. In addition, the bifunctional strategy is postulated to act multifunctionally by cleaving target mRNA, effectively reducing target mRNA concentration, inhibiting target mRNA translation, and sequestering the target mRNA from the translation machinery (p-body) with the potential for delayed degradation, thereby providing an efficient and sustained RNAi mode. Our results are consistent with this hypothesis. These factors could account for the more than 5-log molar difference in applied dose concentration observed between bi-sh-STMN1 and siRNA^{STMN1} to achieve similar tumor cell growth inhibition *in vitro*.

In conclusion, the bi-sh-STMN1 is a novel agent based on the RNAi strategy of purposively targeting gene expression for silencing through both mRNA cleavage and translational repression/p-body sequestration at a significantly lower dose than conventional siRNA and shRNA so as to achieve the same anticancer effectiveness with less potential for exportin 5 and RISC saturation as well as reducing the risk of off-target effects. In addition to structuring a more potent effector, this construct also allows for spatial and temporal control with the use of a single promoter for efficient multiplexing, with an ultimate aim of achieving simultaneous knockdown of multiple key targets in the same cell. Construction of targeting lipoplexes for systemic delivery and further *in vivo* safety, target specific knockdown assessment and assessment of target-dependent anticancer activity are justified.

Conflict of interest

The authors declare no conflict of interest.

Acknowledgements

We gratefully acknowledge the generous support of the Baylor Health Care System Foundation—Lane Newsom Drennan Fund, the Jasper L and Jack Denton Wilson Foundation, the WW Caruth, Jr Foundation Fund of Communities Foundation of Texas, Merkle Family Foundation and the Mary Crowley Cancer Research Centers. We would also like to acknowledge Brenda Marr and Susan Mill for their competent and knowledgeable assistance in the preparation of this paper.

References

1 Irvine DV, Zaratiegui M, Tolia NH, Goto DB, Chitwood DH, Vaughn MW *et al*. Argonaute slicing is required for heterochromatic silencing and spreading. *Science* 2006; **313**: 1134–1137.
2 Bailis JM, Forsburg SL. RNAi hushes heterochromatin. *Genome Biol* 2002; **3**: Reviews1035.
3 Chu CY, Rana TM. Small RNAs: regulators and guardians of the genome. *J Cell Physiol* 2007; **213**: 412–419.
4 Ghildiyal M, Zamore PD. Small silencing RNAs: an expanding universe. *Nat Rev* 2009; **10**: 94–108.
5 Grimm D, Kay MA. Therapeutic application of RNAi: is mRNA targeting finally ready for prime time? *J Clin Invest* 2007; **117**: 3633–3641.
6 Gewirtz AM. On future's doorstep: RNA interference and the pharmacopeia of tomorrow. *J Clin Invest* 2007; **117**: 3612–3614.
7 Silva J, Chang K, Hannon GJ, Rivas FV. RNA-interference-based functional genomics in mammalian cells: reverse genetics coming of age. *Oncogene* 2004; **23**: 8401–8409.
8 Wang S, Shi Z, Liu W, Jules J, Feng X. Development and validation of vectors containing multiple siRNA expression cassettes for maximizing the efficiency of gene silencing. *BMC Biotechnol* 2006; **6**: 50.
9 Liu YP, Haasnoot J, ter Brake O, Berkhout B, Konstantinova P. Inhibition of HIV-1 by multiple siRNAs expressed from a single microRNA polycistron. *Nucleic Acids Res* 2008; **36**: 2811–2824.
10 Li L, Lin X, Khvorova A, Fesik SW, Shen Y. Defining the optimal parameters for hairpin-based knockdown constructs. *RNA (New York, NY)* 2007; **13**: 1765–1774.
11 Pillai RS. MicroRNA function: multiple mechanisms for a tiny RNA? *RNA (New York, NY)* 2005; **11**: 1753–1761.
12 Zeng Y, Cai X, Cullen BR. Use of RNA polymerase II to transcribe artificial microRNAs. *Methods Enzymol* 2005; **392**: 371–380.
13 Nemunaitis J, Senzer N, Khalil I, Shen Y, Kumar P, Tong A *et al*. Proof concept for clinical justification of network mapping for personalized cancer therapeutics. *Cancer Gene Ther* 2007; **14**: 686–695.
14 Rana S, Maples PB, Senzer N, Nemunaitis J. Stathmin 1: a novel therapeutic target for anticancer activity. *Expert Rev Anticancer Ther* 2008; **8**: 1461–1470.
15 Iancu C, Mistry SJ, Arkin S, Wallenstein S, Atweh GF. Effects of stathmin inhibition on the mitotic spindle. *J Cell Sci* 2001; **114**(Part 5): 909–916.
16 Alli E, Yang JM, Hait WN. Silencing of stathmin induces tumor-suppressor function in breast cancer cell lines harboring mutant p53. *Oncogene* 2006; **26**: 1003–1012.
17 Zhang HZ, Wang Y, Gao P, Lin F, Liu L, Yu B *et al*. Silencing stathmin gene expression by survivin promoter-driven siRNA vector to reverse malignant phenotype of tumor cells. *Cancer Biol Ther* 2006; **5**: 1457–1461.
18 Mistry SJ, Atweh GF. Therapeutic interactions between stathmin inhibition and chemotherapeutic agents in prostate cancer. *Mol Cancer Ther* 2006; **5**: 3248–3257.
19 Ngo TT, Peng T, Liang XJ, Akeju O, Pastorino S, Zhang W *et al*. The 1p-encoded protein stathmin and resistance of malignant gliomas to nitrosoureas. *J Natl Cancer Inst* 2007; **99**: 639–652.
20 Wang R, Dong K, Lin F, Wang X, Gao P, Wei SH *et al*. Inhibiting proliferation and enhancing chemosensitivity to taxanes in osteosarcoma cells by RNA interference-mediated downregulation of stathmin expression. *Mol Med (Cambridge, MA)* 2007; **13**: 567–575.
21 Azuma-Mukai A, Oguri H, Mituyama T, Qian ZR, Asai K, Siomi H *et al*. Characterization of endogenous human argonautes and their miRNA partners in RNA silencing. *Proc Natl Acad Sci USA* 2008; **105**: 7964–7969.

22 Lee Y, Kim M, Han J, Yeom KH, Lee S, Baek SH *et al*. MicroRNA genes are transcribed by RNA polymerase II. *EMBO J* 2004; **23**: 4051–4060.
23 Lagos-Quintana M, Rauhut R, Meyer J, Borkhardt A, Tuschl T. New microRNAs from mouse and human. *RNA (New York, NY)* 2003; **9**: 175–179.
24 Mendell JT. miRiad roles for the miR-17-92 cluster in development and disease. *Cell* 2008; **133**: 217–222.
25 Wu L, Fan J, Belasco JG. Importance of translation and nonnucleolytic ago proteins for on-target RNA interference. *Curr Biol* 2008; **18**: 1327–1332.
26 Matranga C, Tomari Y, Shin C, Bartel DP, Zamore PD. Passenger-strand cleavage facilitates assembly of siRNA into Ago2-containing RNAi enzyme complexes. *Cell* 2005; **123**: 607–620.
27 Leuschner PJ, Ameres SL, Kueng S, Martinez J. Cleavage of the siRNA passenger strand during RISC assembly in human cells. *EMBO Rep* 2006; **7**: 314–320.
28 Pizzorno MC, O'Hare P, Sha L, LaFemina RL, Hayward GS. Trans-activation and autoregulation of gene expression by the immediate-early region 2 gene products of human cytomegalovirus. *J Virol* 1988; **62**: 1167–1179.
29 Soutschek J, Akinc A, Bramlage B, Charisse K, Constien R, Donoghue M *et al*. Therapeutic silencing of an endogenous gene by systemic administration of modified siRNAs. *Nature* 2004; **432**: 173–178.
30 Roush SF, Slack FJ. Micromanagement: a role for microRNAs in mRNA stability. *ACS Chem Biol* 2006; **1**: 132–134.
31 Wu L, Fan J, Belasco JG. MicroRNAs direct rapid deadenylation of mRNA. *Proc Natl Acad Sci USA* 2006; **103**: 4034–4039.
32 Zeng Y, Cullen BR. Sequence requirements for micro RNA processing and function in human cells. *RNA (New York, NY)* 2003; **9**: 112–123.
33 Silva JM, Li MZ, Chang K, Ge W, Golding MC, Rickles RJ *et al*. Second-generation shRNA libraries covering the mouse and human genomes. *Nat Genet* 2005; **37**: 1281–1288.
34 Chen C, Ridzon DA, Broomer AJ, Zhou Z, Lee DH, Nguyen JT *et al*. Real-time quantification of microRNAs by stem-loop RT-PCR. *Nucleic Acids Res* 2005; **33**: e179.
35 McManus MT, Petersen CP, Haines BB, Chen J, Sharp PA. Gene silencing using micro-RNA designed hairpins. *RNA (New York, NY)* 2002; **8**: 842–850.
36 Landthaler M, Gaidatzis D, Rothballer A, Chen PY, Soll SJ, Dinic L *et al*. Molecular characterization of human Argonaute-containing ribonucleoprotein complexes and their bound target mRNAs. *RNA (New York, NY)* 2008; **14**: 2580–2596.
37 Robb GB, Brown KM, Khurana J, Rana TM. Specific and potent RNAi in the nucleus of human cells. *Nat Struct Mol Biol* 2005; **12**: 133–137.
38 Langlois MA, Boniface C, Wang G, Alluin J, Salvaterra PM, Puymirat J *et al*. Cytoplasmic and nuclear retained DMPK mRNAs are targets for RNA interference in myotonic dystrophy cells. *J Biol Chem* 2005; **280**: 16949–16954.
39 Jarve A, Muller J, Kim IH, Rohr K, MacLean C, Fricker G *et al*. Surveillance of siRNA integrity by FRET imaging. *Nucleic Acids Res* 2007; **35**: e124.
40 Chiu YL, Rana TM. siRNA function in RNAi: a chemical modification analysis. *RNA (New York, NY)* 2003; **9**: 1034–1048.
41 Rossi JJ. Expression strategies for short hairpin RNA interference triggers. *Human Gene Ther* 2008; **19**: 313–317.